ROTORCRAFT PERFORMANCE ENHANCEMENTS DUE TO A LOWER-SURFACE EFFECTOR

Robert L. Roedts II, LifePort, Inc., Woodland, WA, USA
Mark D. Maughmer, The Pennsylvania State University, University Park, PA, USA

Abstract

Although the application of advanced structures and intelligent control systems on helicopters has seen a dramatic increase over the past two decades, the overall performance of helicopters, relative to fixed-wing aircraft, has been somewhat stagnant. This is due to many factors, one of them being the lack of innovative aerodynamic devices that can operate in the unique environment of a rotor. Research over the past 20 years has shown that in order to have a performance increase with the rotor, it must adapt to the changing environment around the azimuth. One method of doing this that is being researched is the use of miniature trailing-edge effectors (MiTEs) on the blades of the rotor. MiTEs are an extension of the passive high-lift device, the Gurney flap. Gurney flaps are small flat plates, between 0.5 to 5 percent chord, fitted perpendicular to the airfoil surface at or near the trailing edge of a wing or rotor blade. A MiTE is an active Gurney flap, which can be used to actively control the spanwise and azimuthal lift and moment distributions on a rotor blade. Compared to traditional trailing-edge flaps, which are being explored for the same application, MiTEs have the advantage of very low inertia and actuator loads. MiTEs have been the focus of experimental and validated computational fluid dynamics research and, as a result of these efforts, an unsteady aerodynamic model was created for MiTEs located at the trailing edge. In the present work, this model has been modified to account for MiTEs placed up to 15-percent of chord upstream of the trailing edge. This model has been incorporated into a rotor performance code to predict the effect of MiTEs on rotor performance and explore their ability to extend the flight envelope of the RAH-66 Comanche. With the increased use of transonic airfoils as facilitated through the use of MiTEs on the outboard section of the rotor blades for stall delay, a 15-percent or more increase in the maximum velocity of Comanche is predicted, or an eight-percent increase in the service ceiling could be achieved.

Nomenclature

A_i = coefficients of indicial functions
b_i = exponents of indicial functions
c = airfoil chord length
c_c = chord force coefficient
c_d = sectional drag coefficient
c_{do} = zero lift (viscous) drag coefficient
c_l = sectional lift coefficient
c_m = sectional pitching-moment coefficient about x=c/4
c_N = normal force coefficient
CP_{vl} = lower-surface vortex center of pressure
D, D_p, D_f = deficiency function
e = flap hinge location in semi-chords
f'' = effective trailing-edge separation point
k = reduced frequency = $\omega_{flap}c/2V$
K = noncirculatory time constant
M = Mach number
Re = Reynolds number based on free-stream conditions and airfoil chord
s = non-dimensional time in semi-chords = $2Vt/c$
St = Strouhal number $(\omega_{VS}\,\delta/V)$
t = time, *sec*
T = noncirulatory time constant in s time
T' = noncirulatory time constant in t time
T_l = basic noncirulatory time constant = c/a
T_{vd} = lower surface noncirulatory time constant
V = velocity
X, Y = circulatory deficiency function
x = airfoil abscissa
α = angle of attack relative to airfoil-chord line, deg
α_e = effective angle of attack relative to airfoil-chord line, deg
α' = scaled angle of attack
β = Prandtl-Glauert compressibility factor = $\sqrt{1-M^2}$
Δ = incremental quantity
δ = MiTE deployment height normal to the surface
Φ = indicial response function
ω = angular flap deployment frequency, rad/s

Superscripts

C = circulatory component
I = induced/apparent mass component
V = vortex induced component

Subscripts

flap = refers to flapping
eff = refers to effective
vl = lower surface vortex
GF = refers to Gurney flap
vl = lower surface vortex
VS = refers to vortex streak
+STALL = refers to the maximum lift stall condition
-STALL = refers to the minimum lift stall condition
δ = refers to flap deflection angle
$\dot{\delta}$ = refers to flap deflection rate

1 INTRODUCTION

MiTEs are essentially deployable Gurney flaps. The Gurney flap was first used in 1971 by race car driver Dan Gurney as a means to increase the downward force on the wings. This download is used to increase the traction of the vehicle, thereby increasing cornering speeds.

To gain a better understanding of this new aerodynamic flap, Gurney brought the flap to the attention of McDonnell Douglas aerodynamicist, Robert Liebeck. He

investigated the aerodynamics of the Gurney flap and introduced their application to the aircraft industry. In this investigation, Liebeck hypothesized the flow structure around a Gurney flap as shown in Figure 1, where two counter-rotating vortices form behind the flap and effectively increase the airfoil's camber near the trailing edge.[1]

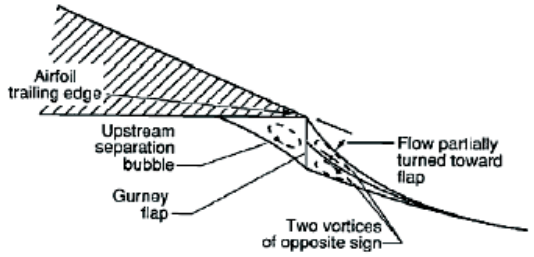

Figure 1: Liebeck's hypothesized flow structure around MiTE.[1]

It has been demonstrated experimentally that Gurney flaps are effective when their height is roughly the same scale as the boundary layer. When the boundary layer is significantly thicker than the flap, there was essentially no effect on the lift of the airfoil.[2] It was postulated in Ref. 5 that the attached counter-rotating vortices act as a means for the airfoil to attain "off-the-surface pressure recovery," allowing for a large discontinuity in the surface pressure at the trailing edge. This effectively shifts the Kutta condition downstream and below the physical trailing edge.

Laser Doppler anemometry (LDA) has been used to detail the flow structures near Gurney flaps.[3] These results display a flowfield that appears to be similar to that of a Kármán vortex street being shed downstream of the Gurney flap that, when time averaged, yields a structure like that hypothesized by Liebeck. The frequency of these oscillations is observed to depend on the height of the Gurney flap and boundary layer thickness.

Miniature trailing-edge effectors, or MiTEs, are a flow control concept that have been considered for use on lifting surfaces.[4,5] Aerodynamically, MiTEs, depicted in Figure 2, have a control effectiveness that is comparable to plain flaps, and high frequency deployments are achievable due to their small size.

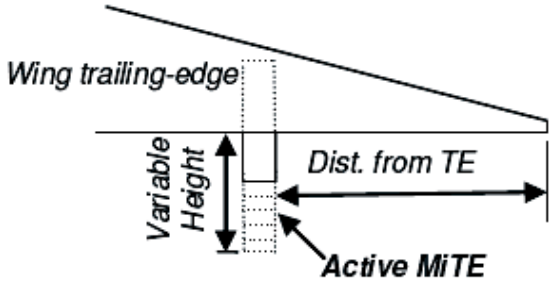

Figure 2: Concept of MiTE[6,7]

Experiments have shown success in their use for flutter stabilization.[5] In this case, they retained their effectiveness at frequencies exceeding 125 Hz. Their use has also been investigated for wind-turbine rotor-blade control.[8] These studies positioned the MiTEs on the upper and lower surfaces of the airfoil upstream of the trailing-edge. This provides aerodynamic control at the outboard stations of the rotorblade that is used for load alleviation in high winds.

1.1.1 Individual Blade Control

For helicopters, vibration reduction is a major area of research in effort to improve the ride qualities over that of current vibration control systems. Methods of higher harmonic control (HHC) and Individual Blade Control (IBC) have been investigated for these applications. The idea behind these concepts is to generate aerodynamic loads at frequencies corresponding to those that are felt in the fuselage and thereby cancel the vibrations. The requirement for these loads is on the order of 4/rev or about 20 Hz. In particular for IBC, active flaps have been considered in numerous studies. MiTEs offer an alternative in that they are able to provide the required changes in lift and moments while offering significantly lower inertia and actuator loads.[7]

1.1.2 Rotor Performance Enhancement

A study has been conducted by Kinzel et al. to investigate the use of MiTEs on rotorcraft.[6,7] The goals of this effort were to first model the aerodynamic characteristics of MiTEs, and then investigate potential rotor performance improvements. This includes increasing the maximum flight speed, achievable rotor thrust, maneuver performance, and payload capabilities. MiTEs can be most beneficial when applied to transonic airfoils, as the airfoil can be tailored for high-speed flow on the advancing side, and the MiTE deployed on the retreating blade when high lift is needed. This can result in increased maximum forward flight speed of the helicopter, as is shown in Figure 3.

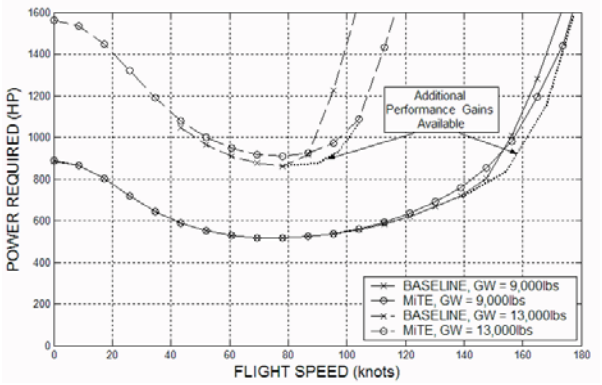

Figure 3: Comparison between baseline and MiTE rotor performance in level forward flight with variations in the gross weight calculated using the dynamic stall model and without an optimal MiTE deployment schedule.[6,7]

All of the performance analyses conducted in this initial research was done on configurations in which MiTEs were placed at the trailing-edge of the airfoil. The study that continues in the following sections extends this research to MiTEs placed upstream of the trailing-edge. Although experiments have shown a slight decrease in the effectiveness of a MiTE when it is moved upstream, this placement is advantageous in that it allows the retracted MiTE to be buried within the airfoil.

2 EXPERIMENTAL AND CFD INVESTIGATIONS

The first experiment conducted by the Penn State research team that of a two-dimensional airfoil tested in a

wind tunnel with and without Gurney flaps attached at and near the trailing edge.[9] The baseline airfoil was initially tested, then measurements were made with Gurney flaps of 0.005c, 0.01c and 0.02c in height located on the lower surface at chord-wise locations of 0.9c, 0.95c and 1.0c. All of these configurations were tested with natural and fixed transition, a chord Reynolds number of 1.0 x 10^6, and a Mach number of less than 0.2. Figure 4 shows the effect of a Gurney flap on $c_{l,max}$ in terms of its height and location.

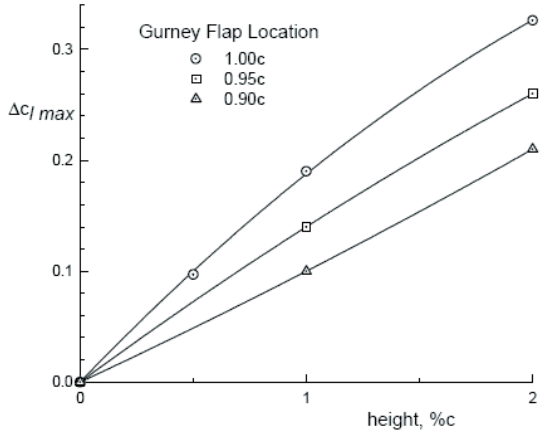

Figure 4: Change in maximum lift coefficient with varying Gurney flap heights and chordwise locations[9]

To further the understanding of Gurney flaps, a second wind tunnel experiment was conducted of an oscillating Gurney-flap equipped VR-12 airfoil tested in the U.S. Army Compressible Dynamic Stall Facility (CDSF) located at the NASA Ames Research Center.[10] The test matrix consisted of an airfoil having a Gurney flap located at the trailing edge and oscillated at reduced frequencies, *k*, of 0.0, 0.05 and 0.1. The Reynolds number ranged from 0.7 x 10^6 to 1.6 x 10^6 and Mach numbers of 0.2, 0.3 and 0.4. The Gurney flap heights investigated were 0.0085c, 0.0135c and 0.024c. Figure 5 shows results from these experiments at Mach numbers of (a) M=0.3 and (b) M=0.4.

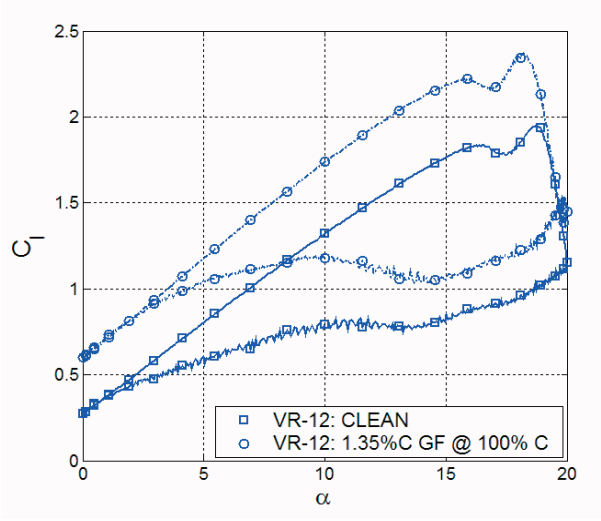

(a) M = 0.3

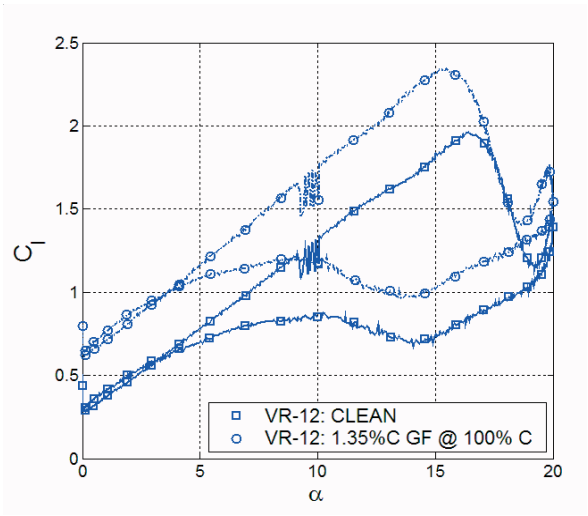

(b) M = 0.4

Figure 5: Comparison of the lift for the VR-12 baseline airfoil and with a 0.0135c height Gurney flap in dynamic stall at a reduced frequency of 0.05[10]

Ideally, more experimental testing would have been done to investigate the performance of MiTEs; however, because of cost and complexity, these tests have yet to be done. This being the case, computational methods have been employed for the initial stages of this research. The NASA CFD code, OVERFLOW2, was validated using the two experiments and used for the analysis of Gurney flaps and MiTEs.[6,7,11] Active deployment computations were performed for MiTEs located at the trailing edge and at 90-percent chord of the airfoil.[7] The differences in visual flow behavior that depend on the MiTE chordwise location can be observed in Figure 6.

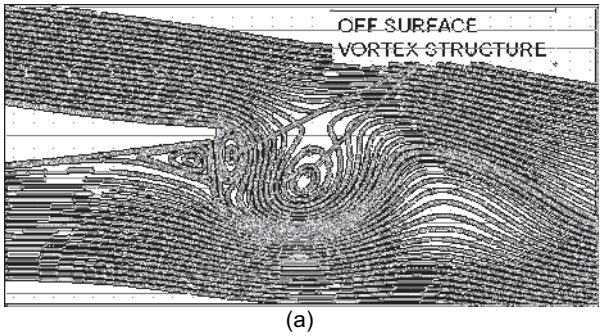

(a)

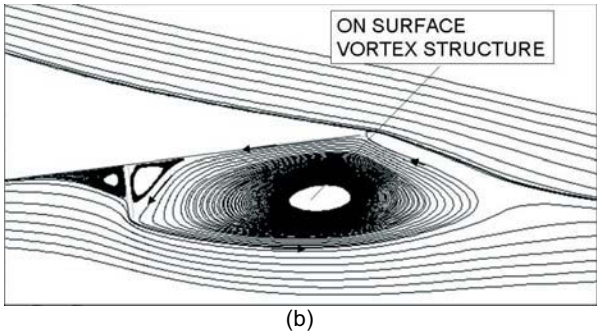

(b)

Figure 6: Comparison of streamlines during deployment at varied MiTE locations when fully deployed.[6]

Figure 7 shows the quantitative differences between a MiTE placed at the trailing edge and at 90% chord.

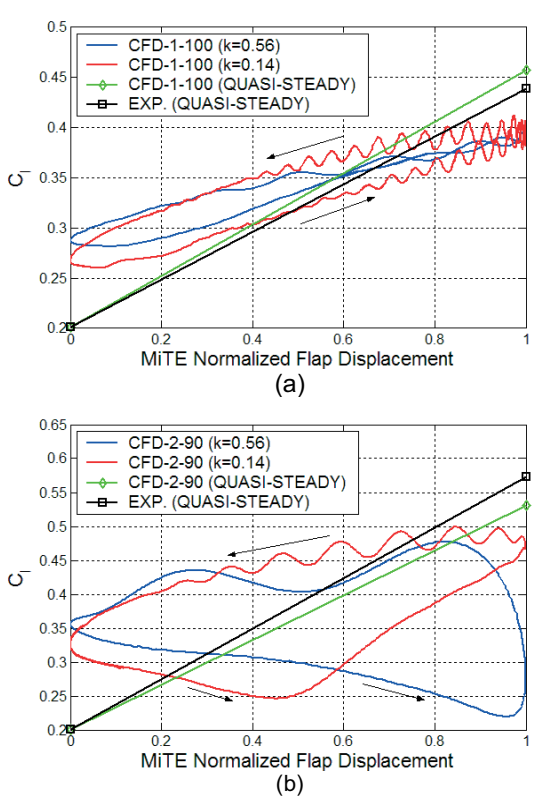

Figure 7: CFD results of deployment with MiTE placed at (a) trailing edge and (b) 90% chord.

3 AERODYNAMIC MODELING

To explore the application of MiTEs to rotorcraft, an analytic aerodynamic model that can produce computationally fast results such that it is suitable to be used in a rotor performance program is desirable. The aerodynamic response of a MiTE depends on frequency, free-stream velocity, Mach number, and angle of attack at which the MiTEs are deployed.[6,7] Since the primary focus of this research is of MiTEs delaying the onset of stall and extending the flight envelope, dynamic stall modeling must be included.

The well-validated Leishman-Beddoes model is used to account for the unsteady aerodynamics and dynamic stall of the oscillating airfoil to which MiTEs are attached. Using OVERFLOW, simulations are performed over a wide range of angles of attack and freestream conditions to predict the static aerodynamic changes due to a Gurney flap. These results are then modified using the Hariharan-Leishman unsteady flapped-airfoil model to predict the unsteady aerodynamics that accompanies a MiTE deployment. This modified Hariharan-Leishman model, along with the Leishman-Beddoes unsteady aerodynamics and dynamic stall models, is used to predict the performance of a MiTE-equipped rotor. Further modifications were made to both the flap and dynamic stall models to account for the behavior of an upstream MiTE.

3.1 Gurney Flap Effects

The effects of a Gurney flap at various Mach numbers and angles or attack forms basis for the aerodynamic model of MiTEs. For simple plain flaps, thin-airfoil theory is used. Due to the sizeable amount separated flow that accompanies Gurney flaps and deployed MiTEs, thin-airfoil theory is unsuitable. Thus, experimental data and/or CFD was used to ascertain the effects of Gurney flaps and MiTEs, which were then used to develop a simplified analytical method for predicting their effects.

When use is made of a scaled angle of attack, α', as given by Eq. (1)

$$\alpha' = \frac{\alpha - \alpha_{-Stall}}{\alpha_{+Stall} - \alpha_{-Stall}} \quad (1)$$

the dependency of Gurney flap performance on Mach number is essentially eliminated[6,7] To account for the changes in the baseline airfoil performance due to a Gurney flap, only the aerodynamic characteristics of the baseline airfoil are required, along with the changes to the aerodynamics due to a Gurney flap at a single Mach number. For this purpose, the baseline airfoil aerodynamics and its Mach number dependency can be obtained experimentally, or generated using any number of two-dimensional airfoil codes.[12]

Based on what experimental data is available, the changes in the lift and moment coefficients determined for a Mach number of zero are set to decrease linearly with increasing Mach number and become zero for a Mach number of 1.0, while the drag increment is set to remain constant. At or below negative stall, the Gurney flap has no effect on lift, drag or pitching moment due to it being submerged in the boundary layer. For positive stall, however, the lift coefficient is taken to gradually increase to a value of 0.7 of that seen in the range of $0.0 < \alpha' < 1.0$. This gain in lift uses an exponential function and then diminishes as the angle of attack approaches 90˚. The drag of the Gurney flap differs slightly as there is an initial decrease after the baseline airfoil stalls. At angles slightly higher than $\alpha' = 1.0$, the drag increment from the Gurney flap is 50 percent of that at positive stall. Exponential functions are used to smooth the effect as drag diminishes to zero as the angle of attack approaches 90˚. An example of Gurney flap aerodynamics that have been generated is presented along with baseline characteristics in Figure 8.

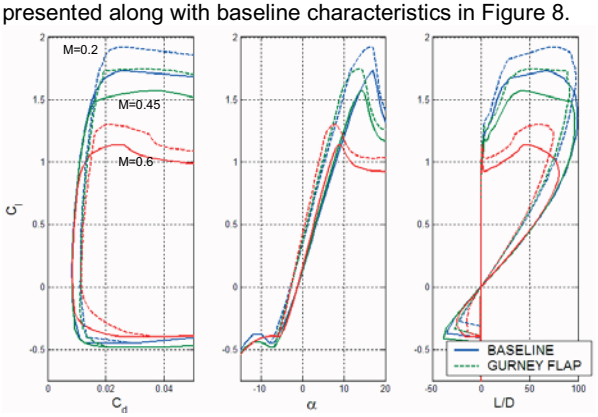

Figure 8: Example airfoil data sets modified to predict the effects of a Gurney flap at various Mach numbers.[7]

3.2 Unsteady Aerodynamic Model

To predict the potential performance of a helicopter, it is necessary to accurately predict the aerodynamics of the rotor system over its entire operational flight envelope. The most difficult and uncertain aspect of this process is the treatment of unsteady aerodynamics. This is especially true when the helicopter is in high-speed forward flight or during flight maneuvers. In the model employed here, the unsteady effects on the oscillating airfoil, as well as dynamic stall, are accounted for using the method developed by Leishman-Beddoes.[13] The unsteady aerodynamics that accompany a MiTE deployment are addressed by adapting the Haraiharan-Leishman flapped-airfoil model.[14,15,16] These models are based on an indicial response, that is, a step change in angle of attack or flap deflection. These results are then generalized to any time histories using a finite-difference approximation to the Duhamel integral.

3.2.1 Leishman-Beddoes Unsteady Aerodynamic Model

The Leishman-Beddoes unsteady aerodynamic model uses indicial response to determine the unsteady effects of an oscillating airfoil.[13] Here, the response to an indicial step in angle of attack is approximated as

$$\phi_\alpha^C(M,s) = 1.0 - A_1 e^{(-b_1\beta^2 s)} - A_2 e^{(-b_2\beta^2 s)} \tag{2}$$

The empirical constants are set to A_1 = 0.3, A_2 = 0.7, b_1 = 0.14, and b_2 = 0.53 as recommend in Ref. 14. The indicial response function given by Eq. (2) is solved using the convolution integral and then discretized to obtain the following deficiency functions that relate to the pitch rate and time history.

$$X_n = X_{n-1}\exp(-b_1\beta^2\Delta s) + \Delta\alpha_n A_1 \exp(-b_1\beta^2\Delta s/2) \tag{3}$$

$$Y_n = Y_{n-1}\exp(-b_2\beta^2\Delta s) + \Delta\alpha_n A_2 \exp(-b_2\beta^2\Delta s/2) \tag{4}$$

These results account for the deficiency of the angle of attack and are used to define an effective attack, α_e, which is given by

$$\alpha_e = \alpha_n - X_n - Y_n \tag{5}$$

Using lookup tables produced from experiment and computational results, the circulatory lift, $c_{l,n}^C(M,\alpha_e)$, is determined. The non-circulatory, or apparent mass, effects are calculated as

$$c_{N,n}^I = \frac{4K_\alpha T_I}{M}\left(\frac{\Delta\alpha_n}{\Delta t} - D_n\right) \tag{6}$$

Where D_n is the deficiency function and T_I is a time constant, both of which are defined in Ref. 13. The time constant represents the non-dimensional time required for pressure disturbances to propagate along the chord length of the airfoil. Finally, the factor K_α depends on the Mach number and defined in Ref. 13.

3.2.2 Leishman-Beddoes Dynamic-Stall Model

A major concern of rotorcraft operation and a factor that limits the flight envelope is dynamic stall. This is caused by the large increases in angle of attack that can occur in high speed forward flight. Since MiTEs can be employed to alleviate retreating blade stall, the modeling of their aerodynamic characteristics in dynamic stall is of great interest.

Figure 9 shows the aerodynamic and flow characteristics of dynamic stall in several stages. On the left are the force and moment trends during dynamic stall while the corresponding flow stages are shown on the right. A notable characteristic of dynamic stall is the large increase in $c_{l,max}$. This is caused by two mechanisms, the first being lags in the unsteady response of pressure and the boundary layer which in turn cause a lag in separation as the angle attack increases. The second mechanism is seen in stage 2-3, where the leading-edge vortex convects over the upper surface of the airfoil and creates the additional lift. It should be noted, however, that there is a large increase in both drag and pitching moment during this stage. After the vortex convects off the surface of the airfoil, a hard stall occurs along with the flow being completely separated on the upper surface. To model this, the Leishman-Beddoes dynamic stall model is used.[13]

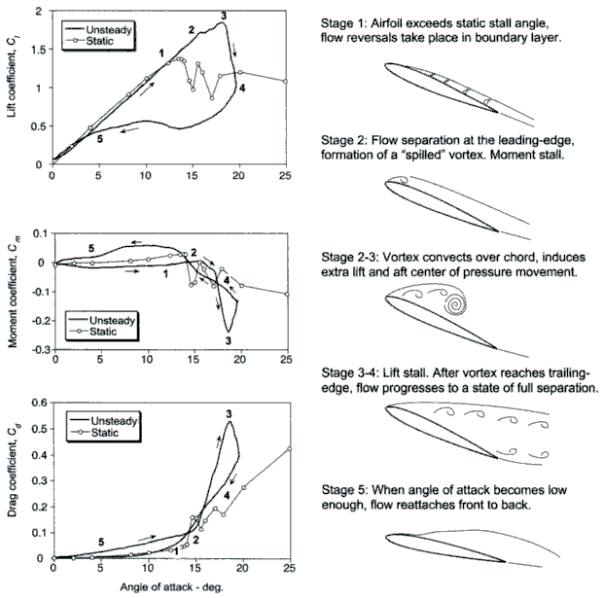

(a) (b)

Figure 9: Force, moment, and flow characteristics of dynamic stall.[17]

The Leishman-Beddoes dynamic-stall model is a semi-empirical method used to predict the dynamic stall characteristics of the baseline airfoils, as well as those fitted with Gurney flaps and MiTEs, in cases where the flow is separated and dynamic stall is occurring.[13] The method utilizes the Kirchhoff/Helmholtz model of the static stall of a flat plate to calculate the lift. The lift is determined as a function of the angle of attack and the effective separation point, *f''*,

$$c_{l,f'',n}^c = c_{l\alpha,n}\left(\frac{1+\sqrt{f''}}{2}\right)^2\left(\alpha_{E^-} - \alpha_z\right) \tag{7}$$

The dynamic stall model also accounts for the leading-edge vortex effects. This vortex is assumed to be fueled by the value of c_v, which is the difference between the linearized normal force lift and the normal force produced in dynamic stall.

(8) $$c^{v}_{N,n} = c^{v}_{N,n}\exp\left(\frac{\Delta s}{T_v}\right) + \left(c_{v,n} - c_{v,n-1}\right)\exp\left(\frac{\Delta s}{2T_v}\right)$$

The vortex decay rate is defined by the time constant T_v, which is a non-dimensional time representative of the time required for the vortex to convect past the trailing-edge of the airfoil. These vortex effects are resolved into lift and drag components and the final lift is determined by superimposing the models using

(9) $$c_{l,n} = c^{C}_{l,n} + c^{I}_{l,n} + c^{v}_{l,n}$$

where $c^{C}_{l,n}$ is defined by Eq. (7) , the apparent mass, $c^{I}_{l,n}$, by Eq. (6), and the vortex lift, $c^{v}_{l,n}$, by Eq. (8). Similarly, the drag is calculated using

(10) $$c_{d,n} = c_{d0} + c^{P}_{d} + c^{I}_{d,n} + c^{v}_{d,n} + c_c$$

Where $c^{v}_{d,n}$ is the drag component of the leading vortex term and the remaining variables are determined by the following equations.

(11) $$c_{d0} + c^{P}_{d} = c_{d,static}\left(\alpha_e, M\right)$$

(12) $$c^{I}_{d,n} = c^{I}_{N,n}\sin\left(\alpha\right)$$

(13) $$c_C = \eta c_{l\alpha}\left(M\right)\alpha_e^2\sqrt{f''}\cos\left(\alpha\right)$$

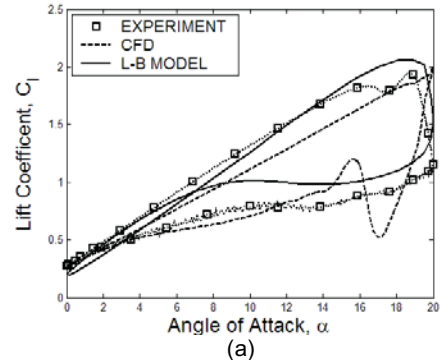

(a)

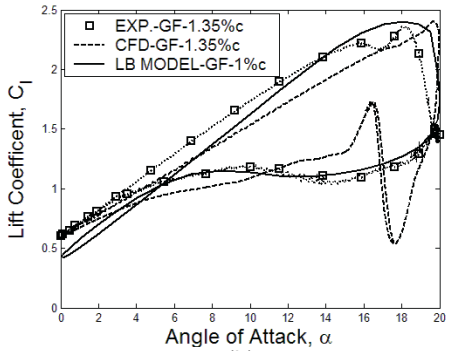

(b)

Figure 10: Results of Leishman-Beddoes dynamic stall model for the VR-12 airfoil with and without a Gurney flap compared with wind tunnel and CFD results.[7]

The models were applied to a baseline VR-12 airfoil, and a VR-12 with a 0.01c height Gurney flap placed at the trailing-edge.[11] These results are shown in Figure 10 Comparing the predictions of dynamic stall with the data from experiment and the CFD shows good agreement. It should also be noted that the magnitude lift is predicted well by the model. These results demonstrate that the dynamic stall model can be extended to Gurney flaps.

3.2.3 Modified Hariharan-Leishman Unsteady Flapped-Airfoil Model

To model the unsteady aerodynamics of MiTEs, the Hariharan-Leishman unsteady flapped-airfoil model is used.[14,15,16] The model incorporates compressibility effects and allows for variable deployment schedules; however, since the model was developed for plain flaps and quasi-steady airfoil theory, it must be modified empirically using CFD results.[6,7,18] Furthermore, for upstream MiTEs, the formation and advection of the vortex that occurs on the lower surface of the airfoil downstream of the MiTE must be taken into account. This is done by use of a vortex model similar to that used in the dynamic stall model in the previous section.

Using the Hariharan-Leishman flapped-airfoil model, the forces and moments of MiTEs can be predicted. The normal force generated by a MiTE can be defined as

(14) $$c_N(s) = c^{C}_{N}(s) + c^{I}_{N,\delta}(s) + c^{I}_{N,\dot{\delta}}(s) + c^{I}_{N}(s)$$

Where $c^{C}_{N}(s)$ is the circulatory load, $c^{I}_{N,\delta}(s)$ and $c^{I}_{N,\dot{\delta}}(s)$ are the apparent mass effects associated with the deployment of the MiTE, and $c^{I}_{N}(s)$ is the load due to the vortex formation and advection on the lower surface on the airfoil that is due to the MiTE deployment and retraction. The first two components are given by

(15) $$c^{C}_{N}(s) = \Delta c_{N,GF}\delta_{eff}(s)$$

(16) $$c^{I}_{N,\dot{\delta}}(s) = \frac{2(1-e_{eff})}{M}T^{'}_{N\dot{\delta}}(K^{n}_{N\dot{\delta}} - K^{'n}_{N\dot{\delta}})$$

where

(17) $$\delta_{eff}(s) = \delta^{n} - X^{n}_{1} - Y^{n}_{1}$$

The exposed height of the MiTE at any time n is defined as δ^n, and the variables $X^{n}_{1}, Y^{n}_{1}, T^{'}_{N\dot{\delta}}, K^{n}_{N\dot{\delta}}$, and $K^{'n}_{N\dot{\delta}}$ are deficiency functions that account for the time history of the system and are defined in Ref. 15. The effective plain-flap hinge location is defined as e_{eff} and defined as the length in semi-chords from the mid-chord to the location of the effective flap hinge. This is adjusted to account for an equivalent apparent mass produced by the MiTE. It also should be noted that the constant of A_1, A_2, b_1, and b_2 are not the same constants as those that appear in the dynamic-stall model.

The model must also account for the MiTE deployment rate. This is an apparent mass effect as the surrounding flow is affected depending on the rate of deployment. Here, e_{eff} is used to capture the effects of this rate

(18) $$c^{I}_{N\dot{\delta}}(s) = \frac{(1-e_{eff})^2}{2M}T^{'}_{N\dot{\delta}}\left(K^{n}_{N\dot{\delta}} - K^{'n}_{N\dot{\delta}}\right)$$

where the deficiency functions, $K^{n}_{N\dot{\delta}}$ & $K^{'n}_{N\dot{\delta}}$, and time constant, $T^{'}_{N\dot{\delta}}$, are defined in Ref. 16.

The pitching moment is also modeled using the Hariharan-Leishman flapped-airfoil method. The components of the unsteady pitching moment are given by

(19) $$c_m(s) = c_m^C(s) + c_{m,\dot{\delta}}^I(s) + c_{m,\dot{\delta}}^I(s) + c_m^I(s)$$

Where the first two terms are

(20) $$c_m^C(s) = \Delta c_{m,GF}\delta_{eff,m}(s)$$

(21) $$c_{m,\dot{\delta}}^I(s) = \frac{-(1-e_{eff})(2+e_{eff})}{2M} T_{m\delta}^{'}(K_{m\dot{\delta}}^n - K_{m\dot{\delta}}^{'n})$$

and $\delta_{eff,m}(s)$, the deficiency functions, and time constants are defined in Ref. 16.

As in Eq. (18), the flap rate can be incorporated into the unsteady pitching moment calculations. Yet again, this is an apparent mass effect that depends on the surrounding flow and the rate of deployment of the MiTE.

(22) $$c_{m,\dot{\delta}}^I(s) = \frac{-2(1-e_{eff})^3 + 3(1-e_{eff})^2 + 2(12e_{eff}-4)}{24M} T_{m\delta}^{'}(K_{m\dot{\delta}}^n - K_{m\dot{\delta}}^{'n})$$

where the deficiency functions, $K_{m\dot{\delta}}^n$ & $K_{m\dot{\delta}}^{'n}$, and time constant, $T_{m\dot{\delta}}^{'}$, are defined in Ref. 16. The final term is the additional pitching moment from an upstream MiTE and the lower surface vortex that is produced. This will be discussed in the next section along with the additional normal force that results.

The unsteady drag is given as

(23) $$c_d = c_{d,p} - c_s + \Delta c_{d,GF}\left(\frac{\delta^n}{\delta}\right) + c_{d,n}^I$$

where the pressure drag, $c_{d,p}$, and the leading-edge suction force, c_s, are defined as

(24) $$c_{d,p} = c_N\alpha + \Delta c_{f.eff}(s)\delta_{pf,eff}$$

(25) $$c_s = \frac{2\pi}{\beta}A_0^2$$

where A_0 is defined in Ref. 16. The third term is the additional drag of the MiTE, which is scaled as a portion of the Gurney flap drag. The final term in the equation is the additional drag from the vortex produced from an upstream MiTE.

3.2.3.1 Additional Effects from Upstream MiTEs

To account for the effects of MiTEs located upstream of the trailing edge, the vortex that forms behind the flap and advects downstream must be addressed. To do this, an approach similar to that used to account for the leading-edge vortex in the dynamic-stall model is used.[18] This model accounts for the vortex scrubbing that occurs on the lower surface of the airfoil. The strength of this vortex may be determined using

(26) $$c_{N,n}^{v,I} = c_{N,n}^{v,I}\exp\left(\frac{\Delta s}{T_{v,I}}\right) + \left(c_{v,n} - c_{v,n-1}\right)\exp\left(\frac{\Delta s}{2T_{v,I}}\right)$$

The time constant, $T_{v,I}$, accounts for the vortex decay, and e is the chordwise location of the MiTE.

(27) $$T_{v,I} = T_{vd} + \frac{2\left(1-e\sqrt{f''}\right)}{St} c_{N,n-1}^{v,I}$$

The unknown term, T_{vd}, that is used to determine this time constant is varied to match CFD results. There are also apparent mass effects associated with the vortex that must be accounted for

(28) $$c_{N,n}^{I,I} = \frac{4K_\alpha T_{v,I}}{M}\left(\frac{\Delta\delta}{\Delta t} - D_n\right)$$

Combining the circulatory and apparent mass effects gives the total force effect of the vortex on the lower surface of the airfoil

(29) $$c_N^{vI} = c_{N,n}^{v,I} + c_{N,n}^{I,I}$$

The pitching moment will also be affected by this vortex. Based on methods used in Ref. 14, the center of pressure is formulated as

(30) $$CP_{vI} = 0.20\left[1 - \cos\left(\frac{\pi T_{vd}}{T_{v,I}}\right)\right]$$

Therefore, the pitching moment is

(31) $$c_m^{vI} = -CP_{vI}c_N^{vI}$$

An additional modification to the Hariharan-Leishman unsteady flapped-model that must be made is that the effective plain flap location, e_{eff}, must be adjusted to reflect the location of the MiTE. Using the CFD results, this term is modified empirically as

(32) $$e_{eff} = 0.9\sqrt[3]{e}$$

The formulation of this term should be investigated further, as it has a large impact on the results produced by modified Hariharan-Leishman model.

3.2.3.2 Parameters of Modified Hariharan-Leishman Model

The parameters A_1, A_2, A_3, b_1, b_2, b_3 and e_{eff} that have been discussed are calibrated to match a sinusoidal deployment result.

Table 1: Modified Hariharan-Leishman model parameters for an upstream MiTE[18]

	M	e_{eff}	A_1	A_2	A_3	b_1	b_2	b_3
MiTE Deploys	0.0	0.85	0.30	0.20	0.40	0.20	0.015	1.75
	0.1	0.85	0.39	0.298	0.40	0.20	0.015	1.75
	0.3	0.85	0.38	0.30	0.50	0.50	0.016	1.20
	0.5	0.85	0.38	0.17	1.00	0.17	0.045	1.50
	0.6	0.85	0.50	0.335	1.10	0.32	0.017	1.75
	0.7	0.85	0.60	0.40	1.00	0.50	0.07	1.50
MiTE Retracts	0.0	0.85	0.30	0.20	0.50	0.15	0.02	0.80
	0.1	0.85	0.41	0.302	0.50	0.15	0.02	0.80
	0.3	0.85	0.33	0.25	0.60	0.20	0.03	0.50
	0.5	0.85	0.38	0.17	1.00	0.17	0.045	1.50
	0.6	0.85	0.48	0.328	0.40	0.40	0.035	1.50
	0.7	0.85	0.60	0.40	1.00	0.50	0.07	1.50

This enables the model to achieve a reasonable agreement in various operating conditions. The parameters are further adjusted to fit the intermediate response to an indicial step deployment. Since the flows are fundamentally different during deployment and retraction, two sets of parameters are used. The values used for a MiTE placed upstream of the trailing edge are presented in Table 1.

3.2.3.3 Results of the Modified Hariharan-Leishman Model

The modified Hariharan-Leishman model was tested using a VR-12 airfoil with a MiTE located upstream of the trailing edge. The first case is that of a MiTE placed at 0.90c and having a height of 0.02c. The Mach number was taken to be *0.45* and the reduced frequency *k = 0.10* (1/rev). For comparison, the results of the analytical model are presented, along with those generated using OVERFLOW , in Figure 11.

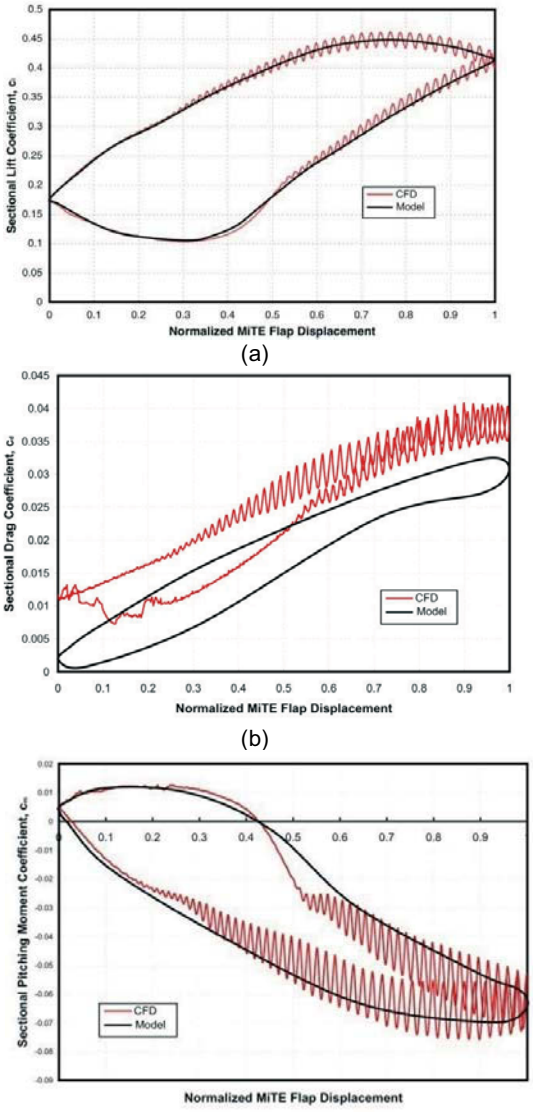

Figure 11: Comparisons between CFD and modified Hariharan-Leishman unsteady flapping model of a 2% MiTE placed at 0.9c for *M=0.45,* α=*0 deg, k=0.10* (a) lift (b) drag (c) moment[18]

In this case, there is good agreement between the CFD and the modified Hariharan-Leishman model in terms of lift and pitching moment. There are however slight discrepancies between the drag predictions, as was seen for the trailing-edge MiTE.

The first case was repeated with the reduced frequency of the MiTE deployment increased to *0.50* (4/rev). The results for this case are given in Figure 12.

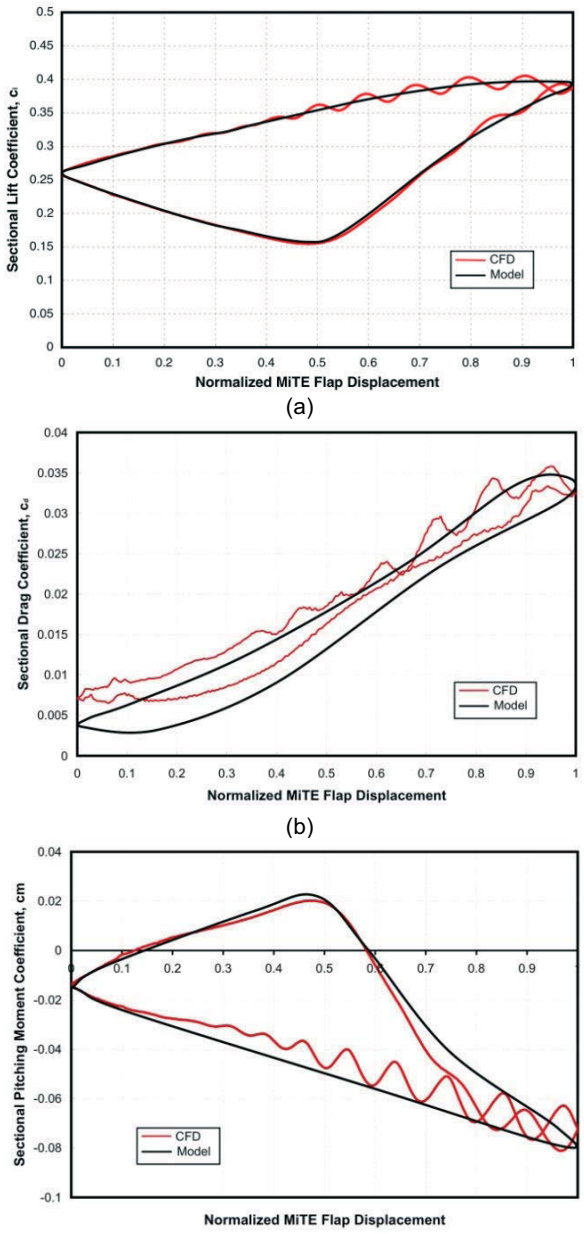

Figure 12: Comparisons between CFD and modified Hariharan-Leishman unsteady flapping model of a 2% MiTE placed at 0.9c for *M=0.45,* α=*0 deg, k=0.50* (a) lift (b) drag (c) moment[18]

Again, there is good correlation between the CFD and the analytical model for the lift and pitching moment and, although less, there is still some discrepancy in terms of drag.

For the next comparisons, the location of the MiTE is also set at 0.85c and 1.00c, the freestream Mach number is *0.4*, and the reduced frequency *1.0.* In addition, the MiTE deployment is now based on a sinusoidal scheme rather than the linear, saw-toothed one of the previous cases. This results in the smoother behavior observed at the endpoints of the deployment cycle. The results of these runs are shown in Figure 13.

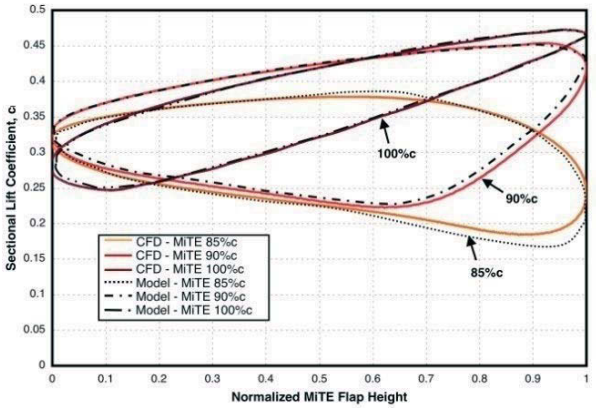

(a)

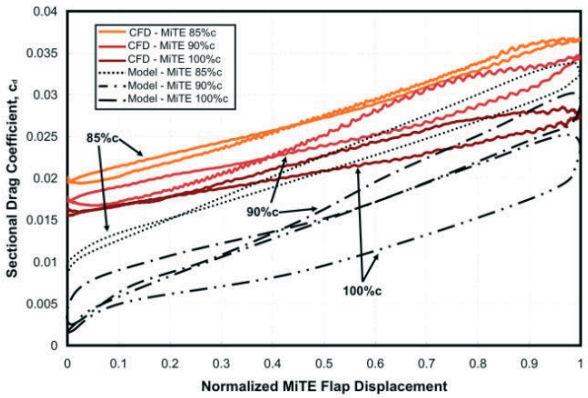

(b)

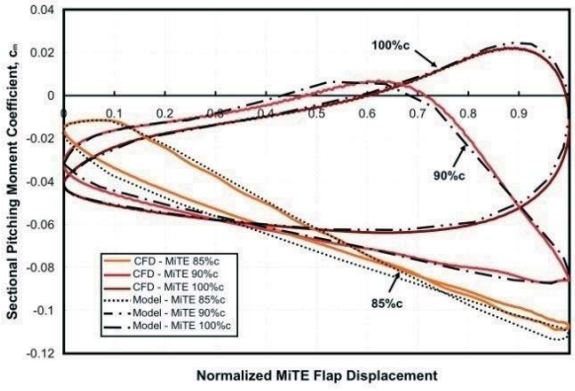

(c)

Figure 13: Comparisons between CFD and modified Hariharan-Leishman unsteady flapping model of a 2% MiTE placed at various locations for *M=0.4,* α*=0 deg, k=1.0* (a) lift (b) drag (c) moment[18]

Again, the agreement between the CFD and the upstream model for the lift and pitching moment coefficients is good, while discrepancies in the drag coefficient remain. This discrepancy, however, is not too significant in that the MiTE drag increment is relatively unimportant to their effect on overall rotor performance, particularly when employed for stall alleviation.

3.3 MiTE Aerodynamic Model

All of the unsteady aerodynamic effects discussed, that is, those due to the pitching airfoil, dynamic stall, and MiTE deployment, can be put together to produce a complete model to predict the aerodynamic behavior of MiTEs. The flowchart presented in Figure 14 is useful for a better understanding of the entire model.

An example of the model predicting all of the unsteady aerodynamics that are integral to it is represented by the case shown in Figure 15.

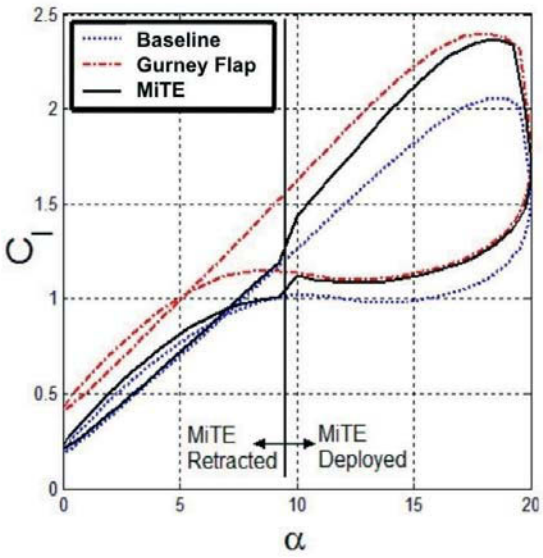

Figure 14: Results of the MiTE Model[6]

Here, the lift curves are shown for an airfoil oscillating through a pitch cycle, including dynamic stall, with a retracted MiTE and one fully deployed. During the pitch oscillation of the airfoil, near 9 degrees angle of attack, the MiTE is deployed, ramping to its full deployment by the time the airfoil angle of attack is 10 degrees. The unsteady aerodynamics of the deployment are captured in how the lift coefficient transitions between the fully retracted and fully deployed curves. In the simple example, the analytical model captures the unsteady lift response due to a deploying MiTE, as well as those due to the oscillating airfoil and dynamic stall.

The comparisons between the analytical model and OVERFLOW results for upstream MiTEs at varying locations, Mach numbers, and reduced frequencies gives confidence that the model can, at least, give a good replication of the CFD results for lift and moment coefficients. The drag predictions obtained using the analytical model do not compare as well with the CFD results because the modified Hariharan-Leishman model fails to fully capture the initial drag rise due to the indicial step deployment of the MiTE. Nevertheless, as the drag increment has been shown to be relatively unimportant in how MiTEs impact overall rotor performance; the overall results are satisfactory and provide confidence that the model is a fairly accurate and efficient method for calculating the aerodynamics of MiTEs.

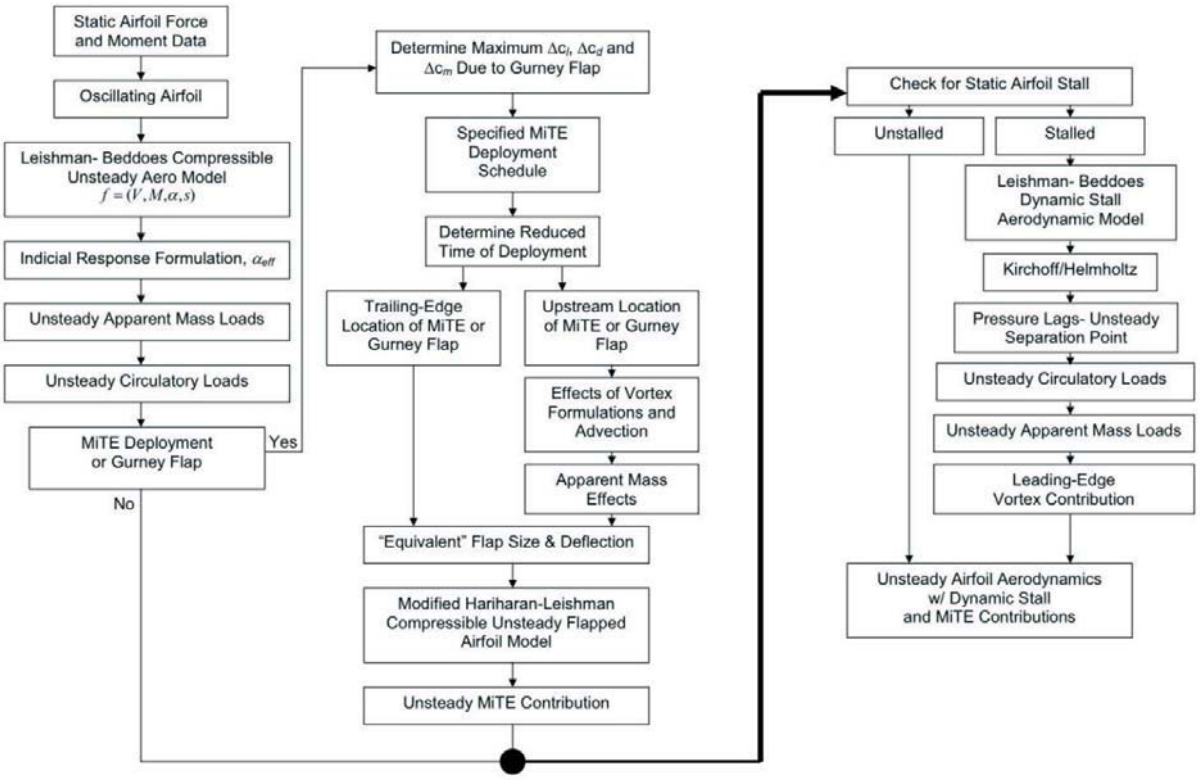

Figure 15: Flowchart of MiTE Aerodynamic Model[18]

4 ROTOR PERFORMANCE

The application of Gurney flaps to helicopter rotors has theoretically demonstrated the potential of increasing the rotor performance at high thrust levels and in forward flight., although it is accompanied by a reduction in performance in low thrust and low-speed flight conditions.[20] With the use of trailing-edge MiTEs, however, which can be deployed and retracted as required, the rotor performance is predicted to increase throughout the flight envelope.[18] These results also suggest the application of MiTEs for further performance gains by optimally tailoring the radial blade loading to reduce induced power, as well as for vibration control. The objective of the research discussed herein, however, is to investigate the possible rotor performance enhancements that gain be achieved using MiTEs positioned upstream of the trailing edge.

4.1 The ROTOR Program

The rotor performance enhancements due to MiTEs are investigated using a modified version of ROTOR, a rotor performance analysis code based on blade-element theory.[21] This program predicts the required power for hover and level forward flight with a trimmed rotor. The rotor is trimmed in the longitudinal and vertical directions, and the pitching and rolling moments are trimmed to zero. This program does not model a tail rotor, so the rotorcraft lateral direction and yawing moment are not considered.

The inflow model used in the computer program is a non-uniform cosine downwash model. Blade flapping with a hinge offset is also modeled, although lead-lag dynamics are neglected. The aerodynamic loads are calculated and then combined with the inertial forces, which are integrated along the span of the blade and around the azimuth to determine the rotor thrust, torque, and power.

4.2 Generation of Airfoil Data Tables

In order for ROTOR to compute the aerodynamic loads, a table of airfoil force coefficients spanning a range of angles of attack and Mach numbers is needed. For MiTE performance calculations, two tables are needed: one for the baseline characteristics and one for the airfoil equipped with a Gurney flap.

The baseline airfoil characteristics were determined through the use of MSES.[12] This provided a consistent set of results over a range of operation of the rotor. It was used to predict c_l, c_d, and c_m for the baseline airfoil from positive to negative stall and at Mach numbers from *0.0* to *1.0*. The sectional characteristics are assumed to be independent of Reynolds number. This is supported by the fact that MSES predicted transition forward of 20 percent chord over most of the operational range. The small difference seen in lift coefficients between natural and fixed transition observed in wind-tunnel tests supports these results. Therefore, transition was set to 2 percent chord on the upper surface and 7 percent on the lower in MSES. With these parameters set,, the data generated using MSES is for the Reynolds number of 4.0×10^6, the average value at blade mid span around the azimuth. To generate the tables for the Gurney flapped airfoils, the Δc_l, Δc_d, and Δc_m quantities obtained using CFD were added to the baseline values at various Mach numbers.

The ROTOR program requires airfoil data at angles of attack ranging from $-180^\circ < \alpha < 180^\circ$. To obtain this needed data beyond positive and negative stall, the airfoil

data from MSES was blended into that of the NACA 0012 airfoil at high angles of attack.[22] In situations where the airfoil is approaching stall and MSES was unable to converge, the Kirchhoff/Helmholtz model is used to predict stall based on a combination of converged predictions and the NACA 0012 data. This sort of situation usually occurs at Mach numbers greater than the critical Mach number. In the analysis of the rotor, these data usually do not have to be implemented, since they would only be required at relatively high Mach numbers on the advancing side of the rotor where the possibility of stall is remote.

4.3 Aerodynamic Models

To model the aerodynamics during the rotor analyses, the models are separated into two categories. The first category is the modeling of the baseline airfoil without a MiTE. There are three different types of models that can be employed: quasi-steady, unsteady, or dynamic stall. The quasi-steady model is based on the airfoil data and the angle of attack is based on the pitch rate, downwash, blade flapping, and other motions. The unsteady aerodynamic model modifies the quasi-steady angle of attack based on indicial methods. For dynamic stall, the Leishman-Beddoes model is used to determine additional unsteady effects, such as lags in the separation and pressure responses, and considers the effects of the leading-edge vortices. In the rotor performance code, the dynamic-stall parameters are based on the experimental data for the NACA 0012 airfoil, since these data are complete and available. This can be done because the separation and pressure time constants, T_f and T_p, are relatively insensitive to the actual airfoil used. For future efforts, determining constants that are more representative of the actual airfoil should be considered.

The second category of aerodynamic models is one that pertains to the modeling of MiTEs. The program is set up to use an additional set of data that is for the same airfoil with a Gurney flap that matches the geometry of the MiTE being used when fully deployed. This provides the needed $\Delta c_{l,GF}$ and $\Delta c_{d,GF}$ as a function of angle of attack and Mach number. The user has the ability to select the steady linear model or the unsteady flapped-airfoil model. The linear model assumes there are no lags and uses linear interpolations between the baseline and the Gurney flap data sets. These interpolations are based on the instantaneous height of the MiTE. The unsteady flapped-airfoil model incorporates the modified Hariharan-Leishman model into the rotor performance code. This model adds the unsteady aerodynamics of a MiTE deployment. If an upstream MiTE is employed, then the unsteady aerodynamics resulting from the formation and advection of vortices on the lower surface of the airfoil are also taken into account.

4.4 MiTE Deployment Scheme

The primary use of MiTEs in this work is to increase rotor performance by means of stall alleviation. The objective is initially to have the MiTE retracted at lower angles of attack when additional lift is not needed, and deployed when it is. The MiTE remains deployed as needed, then retracts when the lift-to-drag ratio drops below that of the baseline airfoil. A typical MiTE deployment schedule is shown in Figure 16.

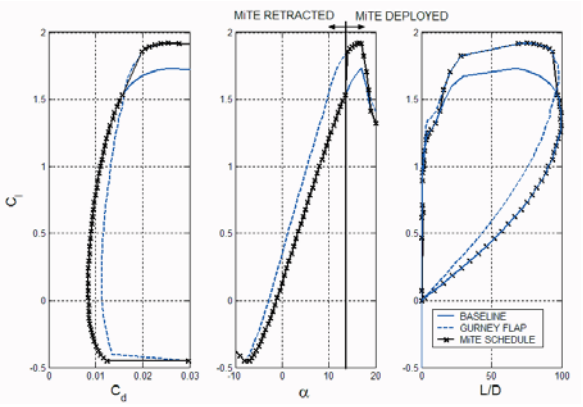

Figure 16: Deployment schedule of MiTEs[7]

When MiTEs are employed, their effect on performance can be predicted by the rotor performance code. The effect of the MiTE as it deploys around the azimuth can be seen in Figure 17. Here, the deployment height of the MiTE is plotted along with the lift coefficient and Mach number.

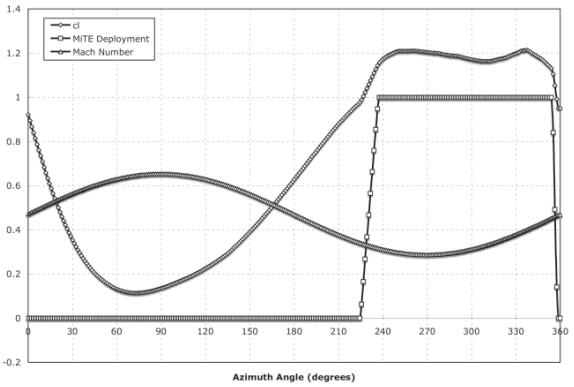

Figure 17: MiTE height and c_l variations around the rotor azimuth[18]

4.5 Rotor Performance Analysis

Table 2: RAH-66 Comanche Characteristics

Parameter	Value
Number of Blades	5
Rotor Diameter	40 ft
Hub Radius	2.5 ft
Hinge Offset	1.5 ft
Blade Chord	1.1 ft
Linear Twist	-8.5 deg
Tip Speed	700 ft/s
Blade Weight	2.9 lb/ft
Equiv. Flat Plate Drag	18 ft^2
Base Weight	10600 lb

The rotor performance comparisons are based on the Boeing/Sikorsky RAH-66 Comanche helicopter. The rotor blades utilize the VR-12 airfoil on the inboard sections and transition to a SSC-A09 airfoil outboard. As the break point between the airfoil sections was not published, it was

assumed to be located at r/R=0.75. Table 2 shows the other parameters of the RAH-66 Comanche used in the performance analysis.

The MiTEs used in these studies are located at 0.90c and have a height of 0.02c. They are also assumed to span the entire span of the blade. The dynamic-stall model and the unsteady flapped-airfoil model are used in performance predictions.

4.5.1 Importance of Unsteady Modeling

In previously done performance predictions of trailing-edge MiTEs, the linear interpolation model was used to determine the effects of MiTEs, since there is only a small difference between it and the unsteady model.[7] As shown in Figure 18, this is not the case with an upstream MiTE, for which the power required by rotor over a range of advance ratios depends somewhat on whether the quasi-steady or unsteady MiTE models are used. This indicates that the unsteady aerodynamic model should be used in order to accurately predict the power required by the rotor.

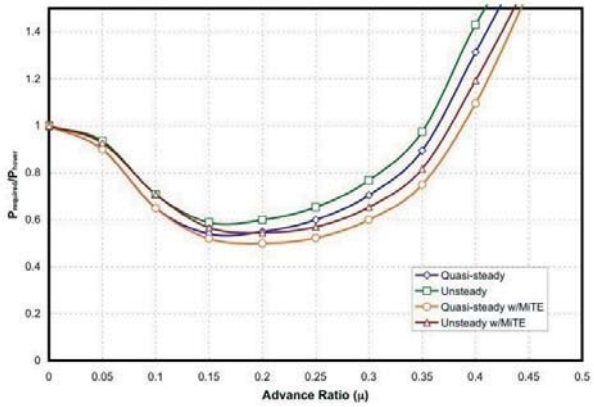

Figure 18: Power Required Comparison[18]

Another aspect of the solution that is affected by the aerodynamic model chosen is that of the prediction of the required MiTE deployment around the azimuth. Figure 19 shows a MiTE deployment schedule for a rotor in high speed flight ($\mu = 0.4$) using the quasi-steady model versus the full unsteady aerodynamic MiTE model. Here, MiTEs are fitted to the outboard airfoil only and deployment is indicated by the shaded region. Again, sizable differences are seen to occur depending on which model is used as to where the MiTE deploys and retracts.

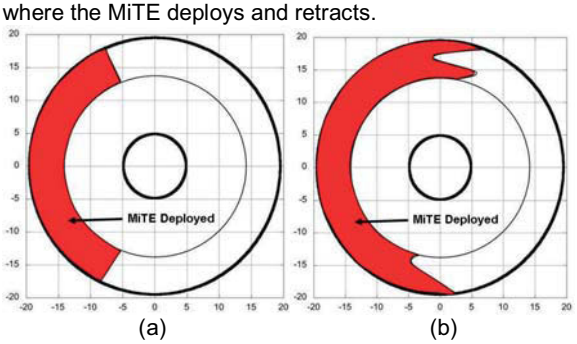

Figure 19: MiTE deployment on rotor disk at $\mu = 0.4$ (a) quasi-steady (b) dynamic stall w/ unsteady MiTE[18]

4.5.2 Pitching Moment Generation

An important concern in considering the practical application of MiTEs is their effect on the pitching moment. In dynamic stall, the pitching moment needs to be kept to a minimum to avoid excessive pitch-link loads. The pitching moment coefficient does increase as MiTEs are deployed, but whether or not the moment exceeds a limiting value depends on the value of the dynamic pressure that occurs over a given region of the rotor. The maximum pitching moment on each side of the rotor over a range of advance ratios are displayed in Figure 20. These values are normalized by the maximum pitching moment on the advancing side of the rotor, which is taken to be the limiting case. It is seen that even with the MiTEs fully deployed in hover, the pitching moment is still lower than the limiting case.

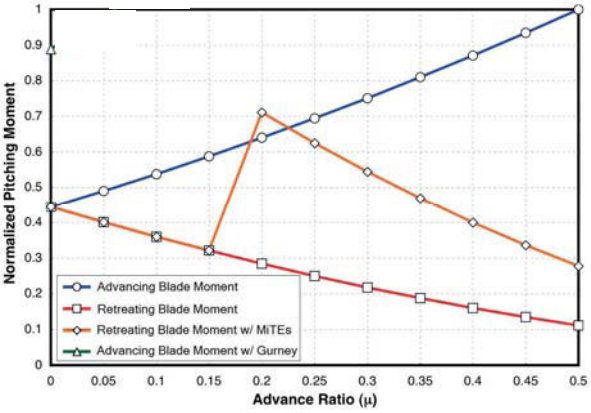

Figure 20: Blade Maximum Pitching Moment[18]

4.5.3 Forward Speed Performance

In previous research, it has been shown that MiTEs have the potential of increasing the maximum forward flight speed of rotorcraft.[6,7] This is consequence of a MiTE's ability to delay stall on the retreating blade. This results in reduced drag and an increased lift-to-drag ratio, allowing for greater speeds. It was also demonstrated that the greatest effect is due to the increased maximum lift on the high-speed airfoil. It was therefore decided to explore changing the radial airfoil distribution on the rotor of the Comanche, making use MiTEs along the span of the blade to increase the lift coefficient when needed.

The effect of forward speed of changing the spanwise airfoil breakpoint for a MiTE equipped blade along with blades not using MiTEs is shown in Figure 21.

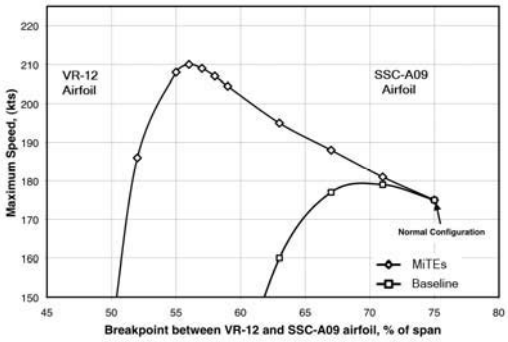

Figure 21: Maximum Speed Increase of the Comanche[18]

Starting at the initial radial transition of r/R=0.75, the use of the SSC-A09 high-speed airfoil was increased by moving the breakpoint inboard. This greater use of the high-speed airfoil reduced the compressibility drag on the advancing blade, while stall was alleviated on the retreating blade through the use of the MiTEs. As a consequence of reduced retreating blade stall, the maximum speed is seen to increase from 175 kts to 210 kts before decreasing again. This shows a possible increase of more than fifteen-percent in the maximum forward speed of the Comanche.

4.5.4 Maximum Altitude Performance

Another scenario for increased performance involves the increased spanwise use of the inboard airfoil, the VR-12, along with full span MiTEs. In this case, an increase the service ceiling of the Comanche helicopter occurs. The same method was used as in the maximum speed case, where the radial transition point is moved on the rotor blade. This time however, instead of moving the transition point inboard, its moved outboard.

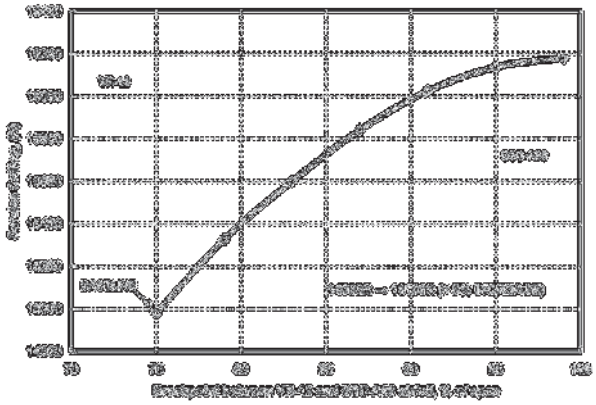

Figure 22: Service Ceiling Increase of Comanche[18]

Here, the rotor benefits from the additional c_l from both the airfoil and the MiTE. As expected, the radial distribution moves outboard to the tip. The service ceiling increased from 14,980 ft to 16180 ft, an increase of eight-percent.

4.6 Discussion of Potential Developments

Although the gains in performance predicted here are significant, there is potential the even greater ones might be achieved. One possibility for performance gains through the use of MiTEs is to integrate them into the rotor design from the onset. All of the situations analyzed in this research used existing rotors, although the preliminary investigations presented here have demonstrated how MiTEs can provide much greater flexibility in determining the airfoil distribution along the span of the blade. This most certainly offers some interesting possibilities for improving rotor performance.

Another potential area of improvement is in the design of airfoils used on the rotor blades. MiTEs offer some interesting possibilities in better tailoring the airfoil design to its operational requirements. For example, by building on some of results presented here, and airfoil could be designed without compromise for the transonic region of the advancing blade. A MiTE could then be used to give this airfoil suitable high-lift performance on the retreating side of the rotor. Thus, MiTEs offer a relatively easy way in which to take advantage of variable geometry.

It is also anticipated that the MiTE deployment scheme could be optimized. In this work, the scheme used was that of deploying when a higher lift coefficient was required to avoid stall and retracting once the lift-to-drag ratio became less than that of the baseline airfoil. While this scheme is simple and intuitive, it is also somewhat arbitrary. Certainly better performance will result when the deployment scheme is better determined.

Finally, it should be noted that other research efforts are underway to tailor the spanwise lift over the blade to produce an optimal distribution and thereby reduce the induced power requirements. This application requires a deployment scheme that is capable of partial deployments, something that is certainly attainable.

5 SUMMARY

The use of upstream MiTE was investigated for the performance enhancement and extension of the flight envelope for rotorcraft. Using the rotor performance code ROTOR, the importance of unsteady aerodynamic modeling was shown by the difference in power requirements between the models. Furthermore, the difference in MiTE deployment was shown with the unsteady case having greater use of MiTEs over the azimuth of the rotor disk. The issue of increased pitching moment on the blades due to MiTE deployment was shown not to be an issue. This was shown by that the fact the pitching moment increase due to MiTEs is less than that of the baseline airfoil on the advancing blade during high speed flight.

As for performance enhancements, the RAH-66 Comanche helicopter was used here as representative. It was shown that using MiTEs and altering the airfoil distribution on the rotor yielded large increases in maximum speed. An increase of eight-percent in the service ceiling was achieved by again altering the airfoil distribution, along with the use of MiTEs. Further performance gains are possible by a number of methods, such as considering the use of MiTEs from the onset of airfoil and rotor design, or even more simply, by optimizing the MiTE deployment scheme.

References

[1]Liebeck, R.H., “Design of Subsonic Airfoils for High Lift,” Journal of Aircraft, Vol. 15, No. 9, September 1978, pp547-561.

[2]Giguére, P., Lemay, J., and Dumas, G., "Gurney Flap Effects and Scaling for Low-Speed Airfoils," AIAA Paper 95-1881, 13th AIAA Applied Aerodynamics Conference San Diego, June 1995.

[3]Jeffrey, D., Zhang, X., and Hurst, D.W., “Aerodynamics of Gurney Flaps on a Single-Element High-Lift Wing,” Journal of Aircraft, Vol. 37, March-April 2000, pp. 295-301.

[4]Lee, H. and Kroo, I.M., "Computational Investigation of Airfoils with Miniature Trailing Edge Control Surfaces ," AIAA Paper 2004-1051, January 2004.

[5]Bieniawski, S. and Kroo, I.M., “Flutter Suppression Using Micro-Trailing Edge Effectors,” AIAA Paper 2003-1941, 2003.

[6]Kinzel, M., Maughmer, M.D. and Lesieutre, G.A., "Miniature Trailing-Edge Effectors for Rotorcraft Performance Enhancements," *Journal of the American Helicopter Society,* Vol. 52,(2), April 2007, pp. 146-158.

[7]Kinzel, M. “Miniature Trailing-Edge Effectors for Rotorcraft Applications," M.S. Thesis, Department of Aerospace

Engineering, Penn State University, University Park, PA, Aug. 2004.
[8]Standish, K.J. and van Dam, C.P., “Computational Analysis of a Microtab-Based Aerodynamic Load Control System for Rotor Blades,” American Helicopter Society Aeromechanics Specialists' Conference, San Francisco, CA, January 2004.
[9]Maughmer, M.D. and Bramesfeld, G., “An Experimental Investigation of Gurney Flaps.” *Journal of Aircraft*, Vol. 45, No. 6, pp. 2062–2067, Nov.–Dec. 2008.
[10]Martin, P.B., McAlister, K..W., Chandrasekhara, M.S., and Geissler, W., "Dynamic Stall Measurements and Computations for a VR-12 Airfoil with a Variable Droop Leading Edge," AHS 59th Forum and Technology Display, Phoenix, AZ, May 2003.
[11]Kinzel, M.P, Maughmer, M.D, Lesieutre, G.L. and Duque, E.P.N, “Numerical Investigation of Miniature Trailing-Edge Effectors on Static and Oscillating Airfoils,” AIAA Paper No. 2005-1039, 2005.
[12]Drela, M., “A User's Guide to MSES 3.04,” Cambridge, MA, Sept. 2002.
[13]Leishman, J.G. and Beddoes, T.S., "A Semi-Empirical Model for Dynamic Stall," Journal of the American Helicopter Society, Vol. 34, No. 3, July 1989, pp. 3-17.
[14]Hariharan, N. and Leishman, J. G., “Unsteady Aerodynamics of a Flapped Airfoil in Subsonic Flow by Indicial Concepts,” *Journal of Aircraft*, Vol. 33, No. 5, Sep.-Oct. 1996, pp. 855 868.
[15]Leishman, J.G., "Unsteady Lift of a Flapped Airfoil by Indicial Concepts," *Journal of Aircraft*, Vol. 31, No. 2, March-April. 1994, pp. 288-297.
[16]Hariharan, N., “Unsteady Aerodynamics of a Flapped Airfoil in Subsonic Flow Using Indicial Concepts,” M.S. Thesis, Department of Aerospace Engineering, University of Maryland, 1995.
[17]Leishman, J. G., *Principles of Helicopter Aerodynamics*, 2nd Edition, Cambridge University Press, New York, NY, 2006.
[18]Roedts, R., “Rotorcraft Performance Enhancements Due to A Lower-Surface Effector,” M.S. Thesis, Dept. of Aerospace Engineering, Penn State University, University Park, PA, August 2008.
[19]Johnson, W., “Rotorcraft Aerodynamic Models for Comprehensive Analysis,” presented at the AHS 54th Annual Forum, Washington, DC, May 1998.
[20]Kentfield, J.A.C., “The Potential of Gurney Flaps for Improving the Aerodynamic Performance of Helicopter Rotors,” AIAA International Powered Lift Conference, pp. 283-292, AIAA Paper 93-4883, 1993.
[21]Hartwich, R., “Parametric Study for the Design of Advanced Rotorcraft Airfoils,” M.S.Thesis, Dept. of Aerospace Engineering, Penn State University, University Park, PA, December 1999.
[22]Critzos, C.C., Heyson, H.H., and Boswinkle, R.W., “Aerodynamic Characteristics of NACA 0012 Airfoil Section at Angles of Attack from 0° to 180°,” NACA TN 3361’ 1955.